Performance of the ALICE Diffractive detector in a beam-test.

Solangel Rojas Torres[a], Ildefonso León Monzón[a], Carlos Duarte Galvan[a], Lucina Gabriela Espinoza Beltrán[a], Juan Carlos Cabanillas Noris[a], Gerardo Herrera Corral[c], Jean-Pierre Revol[d], Christoph Mayer[e], Michal Broz[g], Mario Iván Martínez Hernandez[b], Luís Alberto Perez Moreno[b], Abraham Villatoro Tello[b], Arturo Fernández Téllez[b], Mario Rodríguez Cahuantzi[b], Risto Orava[h,i], Mikael Mieskolainen[h], Alberto Martín Gago Medina[j], Ernesto Calvo Villar[j], Eric Endress[j], Dmitry Finogeev[h], Alexander Kurepin[k], Alexey Kurepin[k], Nikolay Kurepin[k], Andrey Reshetin[k], Arseniy Shabanov[k], Evgueni Usenko[k], Taesoo Kim[f]

[a] *Universidad Autónoma de Sinaloa,CULIACAN, México*
[b] *Benemérita Univ. Autónoma de Puebla,PUEBLA, México*
[c] *Centro de Investigacin y de Estudios Avanzados del IPN, C.D. MÉXICO, México*
[d] *Centro Studi e Ricerche "Enrico Fermi", ROMA, Italy*
[e] *The Henryk Niewodniczanski Inst. of Nucl. Physics Polish Academy of Sciences, CRACOW, Poland*
[f] *Yonsei University, SEOUL, South Korea*
[g] *Czech Technical University of Prague, PRAHA, Czech Republic*
[h] *Helsinki Inst. of Physics, HELSINKI, Finland*
[i] *The University of Helsinki, HELSINKI, Finland*
[j] *Pontificia Universidad Católica del Perú, LIMA, Perú*
[k] *Russian Academy of Sciences, Inst. for Nuclear Research, MOSCOW, Russia*

Abstract

The ALICE Diffractive detector (AD) is a forward detector that was added to ALICE to extend the acceptance of the experiment in the forward rapidity region in order to improve the sensitivity for diffraction physics, for the measurement of the inelastic proton-proton cross-section, and to provide additional measurements of centrality in Pb-Pb, proton-Pb and Xe-Xe collisions. The AD is used as a trigger as well as a beam quality monitor at Point 2 of the LHC. AD consists of two assemblies, ADA and ADC, each station consist of two layers of scintillators. Two detector modules identical to those installed in the experiment were tested in the PS T10 secondary beam at CERN, at beam momenta 1, 1.5, 2 and 6 GeV/c. The purpose was to check the uniformity of the efficiency across the detector modules, and measure the relative response to protons, pions and muons, therefore study the time and charge response. In addition, an attempt was made to obtain an absolute charge calibration of the detector.

Key words: ALICE, Diffractive physics, Performance of High Energy Physics Detectors

Email addresses: rt.solangel@gmail.com,solangel.rojas.torres@cern.ch (Solangel Rojas Torres)

1. Introduction.

ALICE (A Large Ion Collider Experiment) [**?**] is designed to study strongly interacting matter at the highest energy densities reached so far in the laboratory, using proton-proton, proton-nucleus and nucleus-nucleus collisions at the CERN LHC. ALICE tarted operation in 2009, in Run 1 of the LHC, during which studies of diffractive processes in proton-proton collisions were initiated [**?** **?**]. Such studies are based on the ability to define gaps in the pseudorapidity distributions of particles produced in the collisions. It is in this context that the AD detector was proposed, in order to increase the pseudorapidity coverage of ALICE. It was installed around the beam pipe in the forward region; ADC located at 19.5 m from the interaction point (IP) inside the LHC tunnel and ADA situated on the other side at 17 m from the IP of ALICE, behind the compensator magnet on the A-Side [**?** **?**]. Each sub-detector or station is an assembly of two layers segmented in four pads. The pads are made of plastic scintillator coupled at two wavelength shifter bars (at the sides of the pad), they are separated by 0.4 millimeters of air to maximize the light transmission to the WLS bars and collect the light produced inside scintillators. To transport the light of each pad a bundle of 192 fibres (96 for each WLS bar) are coupled to one PMT (Hamamatsu R5946) to convert the light into an electronic signal. A detailed description can be seen in [**?**].

Two AD modules identical to those installed in the experiment were studied in a PS test beam, one ADC and ADA modules, labeled AD1 and AD2 respectively, in order to determine the homogeneity along the pads, sensitivity to a MIP particle and measure the relative response for charge and time of protons, pions and muons at different momentums (1, 1.5,6 and 6 GeV/c).

2. Experimental Setup.

An ADA and ADC pads were tested, these pads are identical to the modules in the experiment, except for the fibres lengths (47 cm in the tested modules). Each bunch of fibres was coupled to a PMT and for the readout we used an electronic system identical to the one installed in ALICE [**?**]. For the beam test the pads were labeled as AD1 and AD2 for ADA and ADC respectively. In addition two scintillator hodoscopes and two Cherenkov radiators were used during the beam test. To study the performance of AD under controlled conditions we use the facilities from T10 [**?**] which delivers secondary particles, mainly pions (π^+) and protons (p^+) produced in the Proton Synchrotron (PS) machine [**?** **?**]. It is possible to adjust the parameters from the beam such like:

momentum of the particles, beam size spot and beam focus. For the beam test we use four different momentum values: 1.0, 1.5, 2.0 and 6 GeV/c, with a resolution of 1.3%.

The setup consists of two different configurations, one used to measure cosmic rays and another for particles from T10 beam. In both cases the nominal voltages were fixed to 1650 and 1500 Volts for AD1 and AD2 respectively. The first setup was placed in order to obtain the MIP position with cosmic rays [**?**], two scintillator hodoscopes, labeled as *Black start* and *Black end*, were placed above and below of AD1 and AD2. The setup for the beam test in T10 is shown in Figure 1. The arrangement is labeled in the beam direction, indicated by the red arrow, and corresponds to: Two hodoscopes, Black-start and Black-end separated by a distance of 1221 cm and two Cherenkov radiators (provided by T0 detector group) labelled as T0-start and T0-end. To readout the signals from all detectors we used a standalone system identical to the Data Acquisition installed in the experiment [**?**]. Is important to point out that the data acquisition was triggered by define a logical `AND` either by the hodoscopes or T0 detectors. The signals passes for a preamplifier that split the signal in to two, one amplified by ten and another by one, that are used by the Front End Electronics (FEE) to measure time and charge respectively.

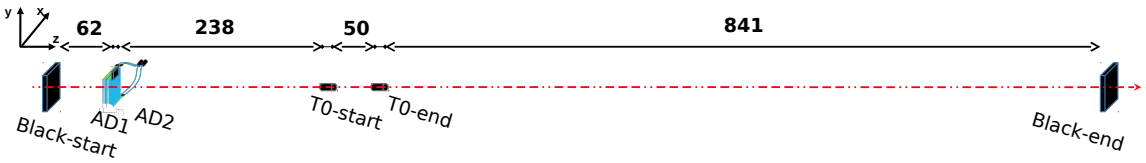

Figure 1: Beam test setup scheme installed at T10 beam line and its separation distances in centimeters. The red arrow show the direction of the beam.

3. Data Samples.

The detector was placed in different positions respect to the beam, the main places are shown in Figure 2. Furthermore, to study the uniformity of charge and efficiency along the components it was necessary to take more runs to complete this analysis. The beam momentum was set at 1 GeV/c for the general study of the components and another set at 1.5, 2 and 6 GeV/c for hitting at the center of the plastic scintillator. Unlike the use of the FEE in the ALICE environment, in T10 a synchronization signal with the particles source is not available, and the events occurs randomly,

therefore we have to define a reference for time, we mainly use T0-end detector to perform that function. Is worth to mention that the signal from the T0s was changed from NIM to TTL level having a constant width and the charge was not measured. The width distribution of the T0-start is not as expected, some events are outside from a narrow distribution; meanwhile the T0-end distribution shows a single narrow peak and to avoid that noise we select the events in a time window between 13 and 17 ns in T0-start.

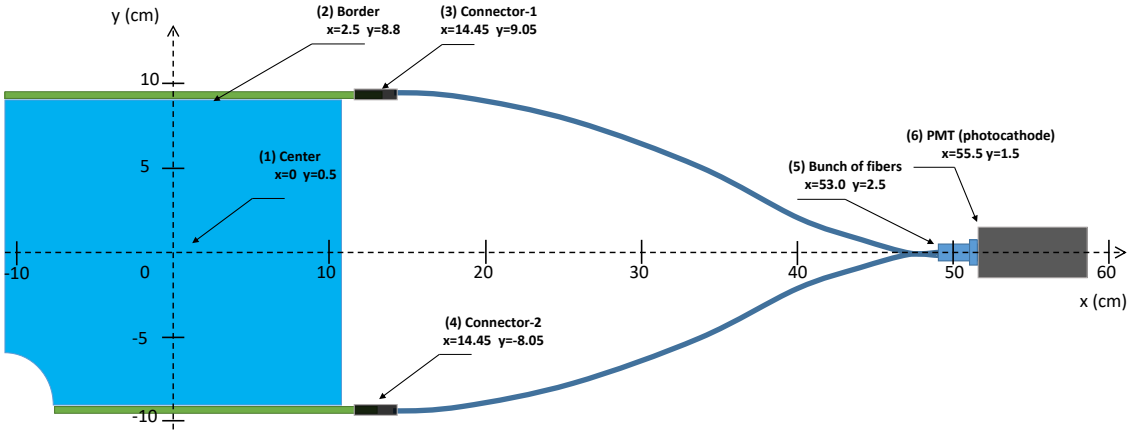

Figure 2: Scheme of positions respect to the plastic scintillator center and beam conditions for the main point of the detector.

All those cleaning criteria were used along in furthers studies. Some other specific cleaning techniques were applied depending on the particular characteristics of the analysis.

4. Results and discussion.

4.1. Cosmic rays measurements.

Using the cosmic setup we measured the charge distribution for a MIP of atmospheric muons. The cosmic particles were selected by a coincidences of the hodoscopes. The results were fitted to a Gaussian plus a Landau functions. The MPV (Most Probable Value) was taken as the position of the MIP, obtaining $Q(AD1) = 8.8 \pm 0.2$ and $Q(AD2) = 7.4 \pm 0.2$ ADC counts. The ratio of the values between AD1 and AD2 will be useful as a correction factor in further analysis.

4.2. Charge and efficiency.

The efficiency is the fraction of events selected according to the equation 1:

$$\text{Efficiency} = \frac{N}{N_{\text{total}}} = \frac{\text{T0-start} \wedge \text{T0-end} \wedge \text{AD}}{\text{T0-start} \wedge \text{T0-end}} \tag{1}$$

where N is the number of events that fulfill the 3-fold coincidence condition and the N_{Total} is the total number of events, given by the 2-fold coincidence of the T0-start and T0-end. To calculate the statistical uncertainty, we used the binomial errors $\delta = \sqrt{N(N-1)/N_{total}}$.

The Figure 3 shows a typical charge distribution of a scan run in the plastic scintillator; the dark gray histogram corresponds to the 2-fold coincidence and the light gray to the 3 fold coincidence. A Landau plus Gaussian function was adjusted to the events detected by the AD module (light gray distribution of Figure 3); the most probable value (MPV) of the fit is used to analyze the homogeneity of the pad.

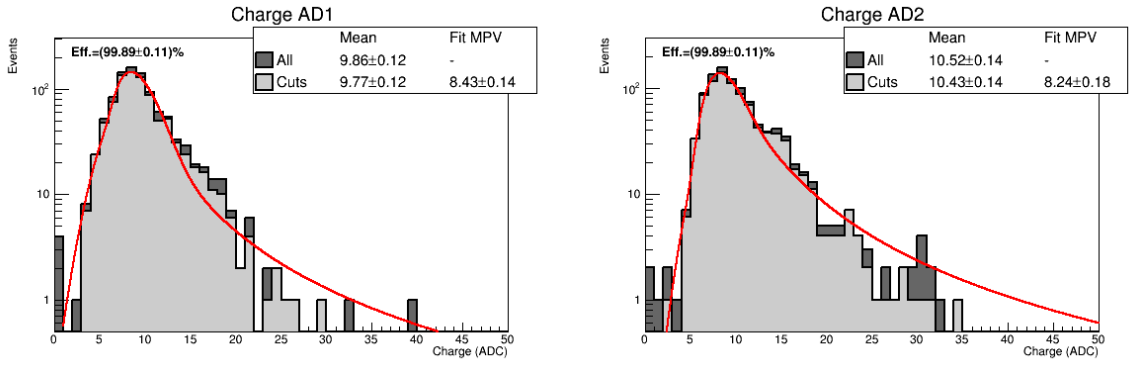

Figure 3: Charge distribution of AD1 and AD2 modules. The dark gray distribution are all the events and the light gray are the selected events by the 3 fold coincidence.

The results of the scans are summarized in the plots of the Figures 4, 5, 6, 7 and 8. The information shown in the plots is: the efficiency of AD1 and AD2 are represented by the green and orange triangles; similarly for the charges, represented by blue circles and red squares. The horizontal scale is the position of the beam respect to the center and the vertical scales at the left and right side are the efficiency and charge respectively. Scans were made along the center of the pads, in vertical and horizontal axis resulting in a uniform efficiency as can be seen in Figure 4 and 5, except at the edges of AD.

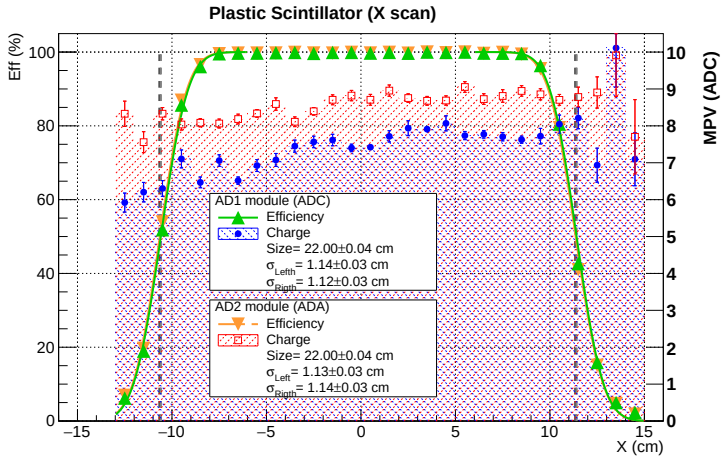

Figure 4: Charge and efficiency obtained in the X-axis scan along the center of the ADs modules.

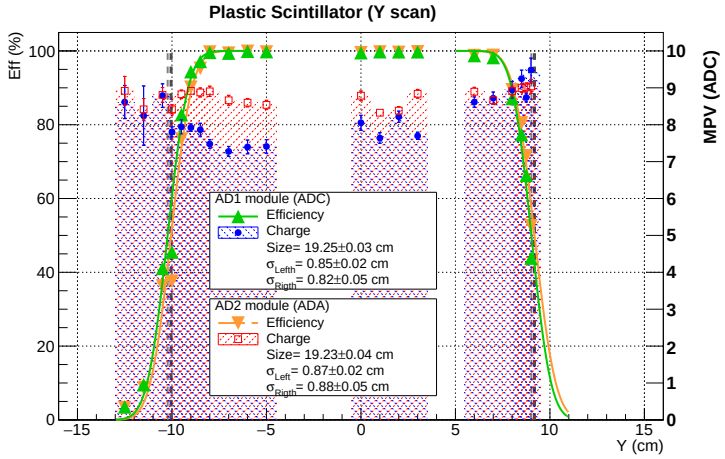

Figure 5: Scan of AD module from the plastic scintillator center along the Y-axis (horizontal). The empty spaces in the plots are skipped measurements.

To estimate the position of the borders and the size of the beam a *Gaussian Cumulative Function distribution* (CDF), shown in the equation 2, was adjusted to the edges of the efficiency plots.

$$F(X|\mu,\sigma) = \frac{1}{\sigma\sqrt{2\pi}} \int_{-\infty}^{X} e^{\frac{-(t-\mu)^2}{2\sigma^2}}\, dt \tag{2}$$

The physical lengths in the vertical and horizontal axes of both modules were calculated using the differences between the distances of the mean values of CDF for each case, obtaining a length of X=22 and Y=19 cm for each axis, that are consistent with the physical length. The size of the beam calculated using the sigmas of the CDF are $\sigma_Y = 1.13 \pm 0.06$ cm and $\sigma_X = 0.86 \pm 0.08$ cm. The scan in the optical connectors demonstrates that the detection probability is very low, the light here is mainly produced by cherenkov effect, that is rapidly absorbed by the optical fibre. The results of the performance of this section can be seen in Figure 6.

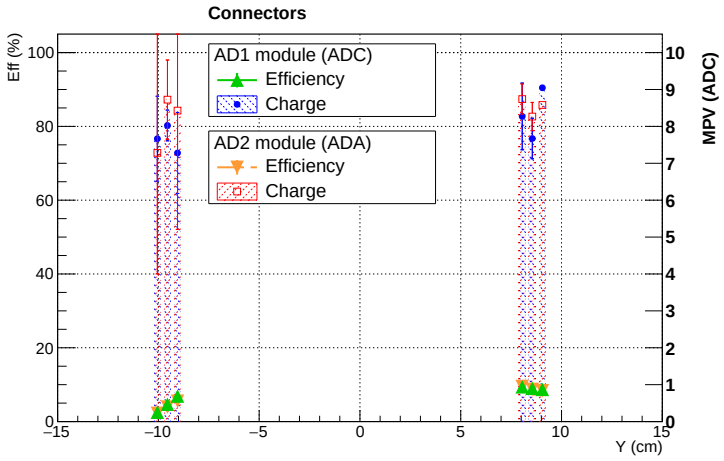

Figure 6: Scan of two optical connectors of the ADA and ADC modules (y-axis scan)

The efficiency when the beam hits in the bunch of fibres (see Figure 7) shows that the detection efficiency is low and a few events are detected. The bunch of fibres is glued in a cylindrical and transparent connector made of acrylic and coupled to the PMT photochathode. Therefore, when a particle hits the connector (∼2.5 cm away from the PMT photochathode) cherenkov light is produced and reach the photocathode of the PMT; if we move the beam in the vertical axis we expect a reduction in the efficiency because there is less material. The charge measured in this section is only due the cherenkov light that reach the photocathode [**?**]. The efficiency along the PMT is reduced when a particle hits far from the photocathode and should produce a signal when impact in the photocathode or the dynodes. This can be seen in Figure 8. The photocathode is placed in the most left side of the plot. As is expected a significant efficiency of 40% is observed when particles hits the PMT photochathode.

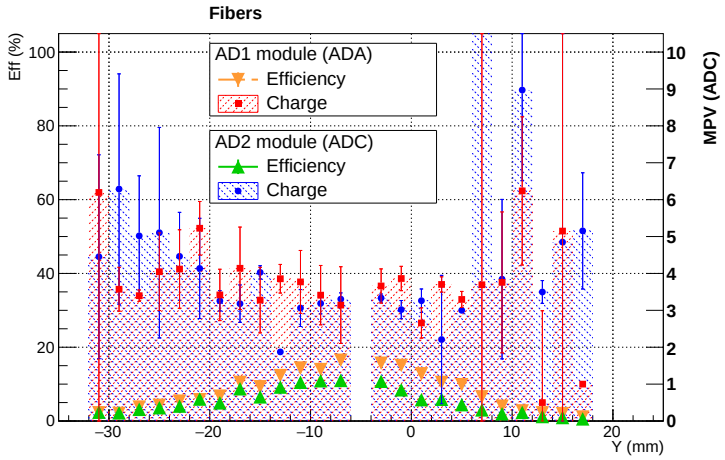

Figure 7: Scan of bunch of fibres for ADA and ADC modules (y-axis scan).

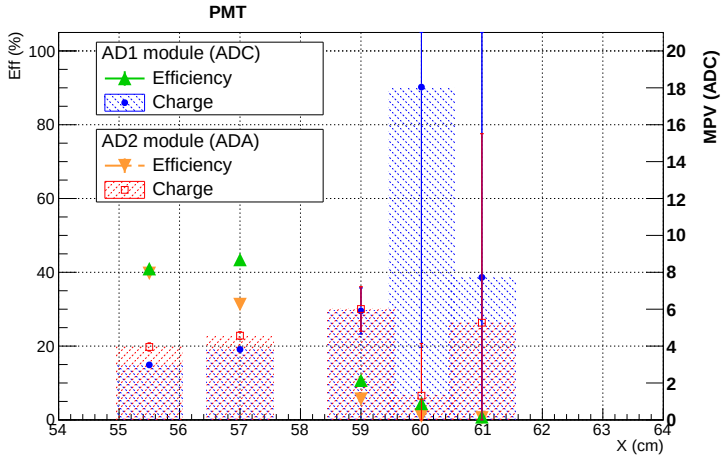

Figure 8: PMT scan for ADA and ADC modules (x-axis scan).

4.3. Time analysis.

To analyze the time response of the detectors, we use all the detectors placed in the setup and define a time reference, given that the particles coming from the PS arrives randomly. The T0-end detector was chosen because of its good time resolution (∼50 ps)[**?**] and the distances respect to other detectors is suitable to distinguish pions and protons using the *Time Of Flight* technique.

For analyze and select particles we used the time differences between the Black-start and T0-end detectors. Two time windows were defined, one to select pions and another for protons. This is shown in Figure 9, pions were selected from 62.0 to 71.5 ns (gray histogram) and protons from 71.5 to 76.0 ns (yellow histogram). This strategy will allow us to identify the particles in other detectors even if the particles are overlapped.

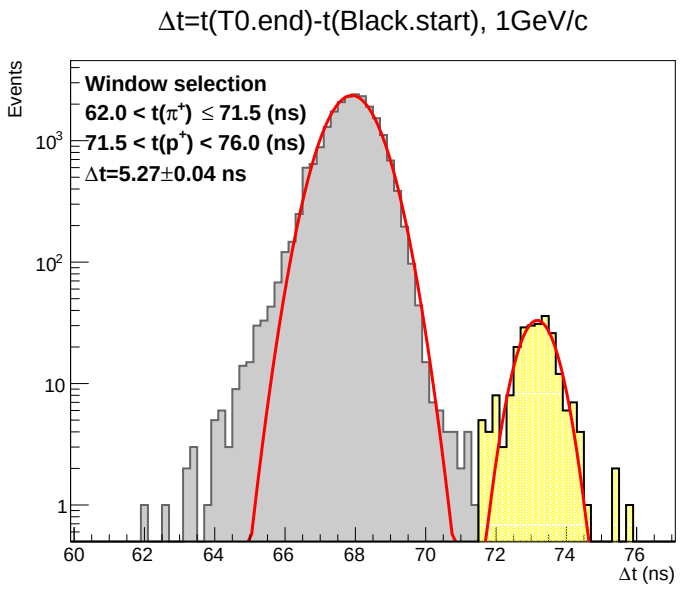

Figure 9: Time window to select pions(gray) and protons(yellow). The time difference between Black-start and T0-end detectors was used, due the good separation and statistic provided by this configuration.

The time measurement are affected by an slewing effect and can be corrected applying the time slewing correction technique to improve the measurement [**?**]. The distribution for pions was selected to make the correction because the effect is clearest. In the Figure 10 can be seen the profile of the time with respect to the charge, represented by the black dots; the behavior can be parametrized according to $t(Q) = p0 + p1 \cdot Q^{p2}$ where $p0$, $p1$, and $p2$ are constants parameters. Once we have obtained the parameters from the fit, the time corrected is calculated subtracting the time $t(Q)$ to the measured time $t(\text{corr.}) = t(\text{measured}) - t(Q)$, where $t(\text{corr.})$ is the time corrected and $t(\text{measured})$ is the time measured of each individual event. The corrected distributions are shown in Figure 11 (bottom histograms), and show how the slewing effect has disappeared. In Figure 11

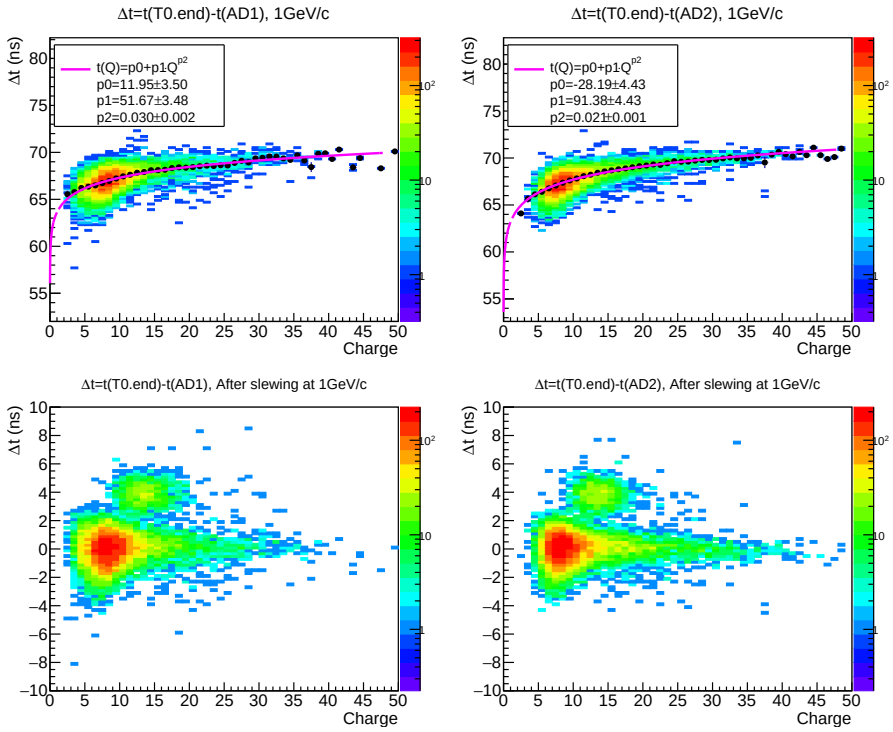

Figure 10: Time slewing correction calculated using the pions distributions of AD1 and AD2 (top row).The corrected distribution was obtained as can be seen in the bottom row.

can be compared the time response of the modules before (top row) and after (bottom row) the slewing correction.

The materials placed along the experimental setup plays an important role in the analysis for particle identification, i.e. to analyze the time and charge properties. AD detector is composed mainly by a piece of *Bicron 404* [**?**] plastic scintillator of 2.5 cm of thickness; the same kind of material is assumed for the Black hodoscopes but with a thickness of 4 cm. The T0 Cherenkov radiators have a more complex composition, and is formed by a 2 cm of thickness quartz radiator [**?**], for the PMT glass of the vacuum tube and the aluminum cover we will consider 1 mm in the front and 1 mm more in the back, and finally the 16 dynodes are made of 0.1 mm thick iron (Fe).

The energy deposited by the particles in the detector is translated to an amount of charge measured, using this we obtained a calibration of the energy deposition in the material. For detectors of moderate thickness x, e.g. scintillators or LAr cells, the energy loss probability distribution is

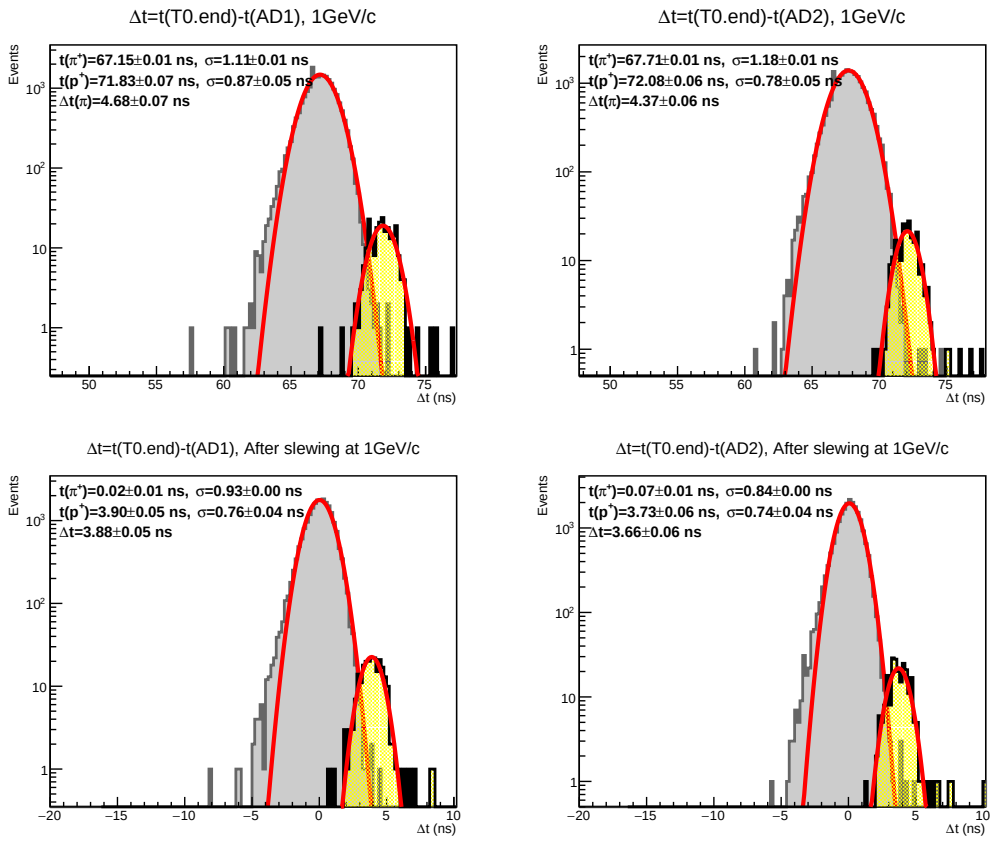

Figure 11: Time distributions of pions (gray) and protons (yellow) at 1 GeV/c beam momentum of ADs detectors before (top row) and after (bottom row) the time slewing correction and the time of flight difference measurements.

adequately described by the highly-skewed Landau (or Landau-Vavilov) distribution [**?** **?**] where the most probable energy loss is:

$$\Delta_p = \xi \left(\ln \frac{2mc^2\beta^2\gamma^2}{I} + \ln \frac{\xi}{I} + j + \beta^2 - \Delta(\beta\gamma) \right) \quad \text{and} \quad \xi = \frac{K}{2}\frac{Z}{A} z^2 (x/\beta^2) \tag{3}$$

The new energy and momentum of the particle was recalculated on each stage using the material budget and $E^2 = p^2c^2 + M^2c^4$. For practical reasons we have defined five stages in the beam setup, which are listed in the Table 1.

The energy loss has been calculated for pions and protons taking into account the material budget of each detector to obtain the new momentum of the particle in each stage. This loss leads

Stage	Placement	Distance (cm)
s0	Before Black-start	-
s1	Black-start to AD1	65.5
s2	AD1 to AD2	3.0
s3	AD2 to T0-start	240.5
s4	T0-start to T0-end	62.0
s5	T0 end to Black-end	854.0

Table 1: Stages: labels, placement and distances traveled by the particles along them. The distances where taken from the middle of each scintillator and the middle of the crystal of the T0s.

to an increase on the time of flight difference between pions and protons which have been calculated for each stage using:

$$t_j = \frac{L}{\beta c} = \frac{L}{p_j c}\sqrt{p_j^2 + m_j^2 c^2} \tag{4}$$

where j indicate the particle (pion or proton for example) and L the distance traveled. The time of flight difference Δt is calculated subtracting the time of flight of two different particles traveling the same distance.

$$\Delta t = t_1 - t_2 = \frac{L}{c}\left[\left(1 + \frac{m_1^2 c^2}{p_1^2}\right)^{1/2} - \left(1 + \frac{m_2^2 c^2}{p_2^2}\right)^{1/2}\right] \tag{5}$$

The results are summarized in the Tables2, 3 and 4 for a momentum of 1, 1.5 and 2 GeV/c respectively. The measurements have a good agreement with respect to the theoretical calculations; and the time slewing correction is improved in comparison with the not corrected data.

A data set was taken at 1.5, 2 and 6 GeV/c momentum and a similar study for 1 GeV/c was done. The selection of particles at 1.5 and 2 GeV/c was made using Black-end instead of Black-start to keep a good separation between pions and proton. At a momentum of 6 GeV/c it was not possible to distinguish pions and protons, due to the small time of flight difference and the overlapping of the two particles distributions. Additionally we obtained a measurement of the time resolution taken from the standard deviation of the Gaussian fit (σ), the information is contained in Table 5. Three different cases were considered for the charge study, the generated by pions, protons and both of them. A Landau plus a Gaussian function was fitted to all cases and the most probable value (MPV) was taken as the charge, this is shown in Figure 12. The results are summarized in

Detector	Distance (cm)	Theoretical Δt (ns)	Δt (ns)	Slewing corr. Δt (ns)
AD1	305.5	4.067	4.68±0.07	3.9±0.05
AD2	302.5	4.030	4.37±0.06	3.66±0.06
T0.start	62.0	0.907	1.18±0.04	-
Black.start	371.0	4.882	5.27±0.04	4.66±0.03
Black.end	845.0	13.438	14.29±0.09	14.5±0.07

Table 2: Distances, theoretical and measured time of flight differences between pions and protons respect to T0-end detector for 1 GeV/c beam momentum. The measured time of flight before and after apply the time slewing correction are in the fourth and fifth columns respectively.

Detector	Theoretical Δt (ns)	Δt (ns)	Slewing corr. Δt (ns)
AD1	1.809	2.03±0.08	1.83±0.09
AD2	1.791	1.2±0.1	1.68±0.08
T0-start	0.394	0.14±0.01	-
Black-start	2.200	2.1±0.03	2.11±0.02
Black-end	5.824	6.12±0.04	6.29±0.03

Table 3: Theoretical and measured time of flight differences of pions and protons respect to the T0-end detector at 1.5 GeV/c beam momentum. The measured time of flight before and after apply the time slewing correction are in the third and fourth columns respectively.

Detector	Theoretical Δt (ns)	Δt (ns)	Slewing corr. Δt (ns)
AD1	1.010	0.72±0.04	0.66±0.04
AD2	1.000	0.14±0.5	0.54±0.04
T0-start	0.218	1.0±0.01	-
Black-start	1.233	1.19±0.02	1.09±0.02
Black-end	3.288	3.21±0.09	3.77±0.01

Table 4: 2 GeV/c beam momentum theoretical and measured time of flight differences between pions and protons respect to the T0-end detector. The measured time of flight before and after apply the time slewing correction are in the third and fourth columns respectively.

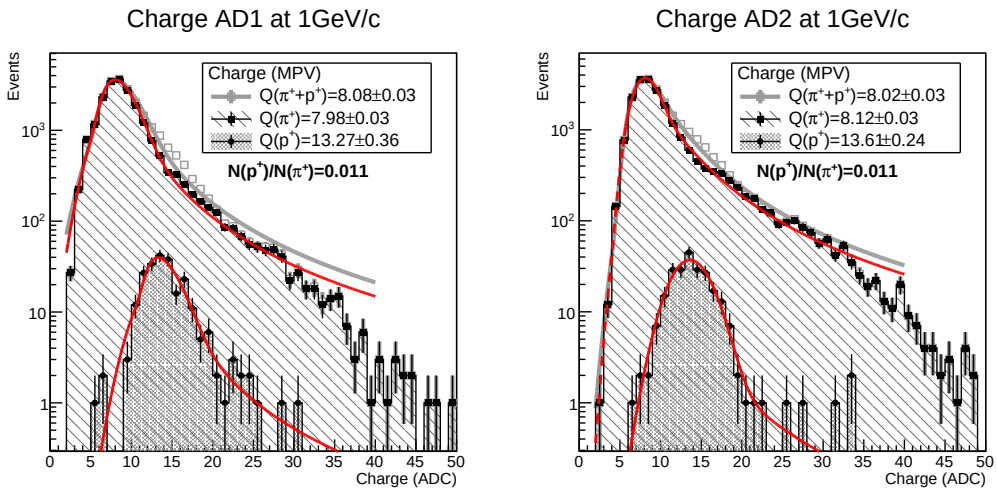

Figure 12: Charges distributions for 1 GeV/c beam momentum for all particles and pions and protons separated.

Momentum	AD1				AD2			
(GeV/c)	σ (ns)		Slewing corr. σ (ns)		σ (ns)		Slewing corr. σ (ns)	
	π^+	p^+	π^+	p^+	π^+	p^+	π^+	p^+
1.0	1.1±0.01	0.87±0.05	0.93±0.01	0.76±0.04	1.18±0.01	0.78±0.05	0.84±0.01	0.74±0.04
1.5	2.5±0.04	1.43±0.06	1.26±0.02	1.18±0.07	3.11±0.06	1.64±0.07	1.17±0.02	1.19±0.06
2.0	2.6±0.02	1.82±0.03	1.32±0.01	1.40±0.04	3.15±0.03	1.84±0.03	1.22±0.01	1.33±0.02
6.0	1.20±0.03		1.12±0.02		1.27±0.03		1.18±0.02	

Table 5: Time resolutions of AD1 and AD2 at different momentum of pions and protons with and without time slewing correction.

the Table 6.

The rest of the sections such as the border, connectors, fibres and PMT were also analyzed, and similarly, the charge response and time resolution were obtained. In the Table 7 are listed the charges and efficiencies corresponding to each section. For hits near to the border a good charge response was obtained but a lower efficiency in comparison to the center of the plastic scintillator. The optical fibres connector and the PMT have a similar charge because some Cherenkov photons are produced in the bunch of fibres near to the PMT and some particles impact directly to the photocathode. For these cases the charge analysis for protons and pions combined is used; the low

Momentum (GeV/c)	AD1			AD2		
	Charge (ADC counts)					
	$\pi^+ + p^+$	π^+	p^+	$\pi^+ + p^+$	π^+	p^+
1.0	8.08±0.03	7.98±0.03	13.27±0.036	8.02±0.03	8.12±0.03	13.61±0.24
1.5	8.3±0.04	8.18±0.04	9.72±0.16	8.56±0.05	8.45±0.05	9.94±0.13
2.0	8.21±0.02	8.12±0.02	8.80±0.06	8.41±0.02	8.35±0.02	8.89±0.06
6.0	7.23±0.09	-	-	7.14±0.08	-	-

Table 6: Charge measured for pions, protons and sum of both. For 6 GeV/c momentum is not possible to distinguish the particles using the time of flight technique.

statistic and efficiencies in most of the run does not allow us to measure separately. Because the amount of protons is small (less than 1%) we can consider only pions.

Section	AD1	AD2	AD1	AD2
	Charge (ADC counts)		Efficiency (%)	
Border	8.42±0.02	9.24±0.01	78.94±0.09	71.6±0.08
Conn. 1	7.01±0.97	6.83±1.08	4.74±0.68	6.19±0.78
Conn. 2	9.70±0.55	9.94±0.72	9.11±0.98	8.68±0.92
Fibres	3.66±0.14	2.14±0.02	10.99±0.15	8.66±0.14
PMT	3.59±0.39	2.56±0.001	38.94±1.06	40.25±1.07

Table 7: Charge and efficiencies of the different sections of the detector.

In the time analysis of the sections (Tables 7 and 8) we obtained, in general, similar resolutions compared with the obtained in the analysis of the center of the plastic scintillator. Furthermore, is of our interest to examine the time difference of the arrival of the signal in those different places, in other words, the time of travel of the photons from certain point to the photocathode. From the results presented in the last two columns of the Table 8 in not easy to distinguish whether the particles hit the connectors, the border or the center, whereas in the PMT and optical fibres is easily seen around 8 ns time difference.

The comparison of the global time resolution (see Table 5) and what is reported in [**?**] (300 and 500 ps in ADA and ADC respectively) do not match; nevertheless the dependency of the time resolution with respect to the charge have been considered. The leading edge trigger produces

Section	AD1: σ (ns)		AD2: σ (ns)		AD1 (ns)	AD2 (ns)
	π^+	p^+	π^+	p^+	Δt (w.r.t. center)	
Center	0.93±0.01	0.76±0.04	0.84±0.01	0.74±0.04	0± 0.01	0±0.01
Border	0.89±0.01	0.83±0.02	0.81±0.001	0.85±0.03	0.19±0.03	0.6±0.01
Conn. 1	1.17±0.2	0.95±0.3	1.54±0.26	0.43±0.14	-0.27±0.92	0.55±0.32
Conn. 2	0.75±0.7	0.37±0.13	1.27±0.12	0.56±0.2	-0.1±0.44	0.82±0.15
Fibres	0.81±0.02	-	0.99±0.3	-	7.97±0.01	7.25±0.05
PMT	0.68±0.03	-	0.89±0.05	-	8.47±0.01	7.77±0.07

Table 8: Time resolution after the time slewing correction and time difference of the signal generated in each section with respect to the center of the AD module. The fibres and PMT sections does not have detection of protons.

the so-called time walk [**?**], and introduce a fluctuation in the crossing time of the threshold. A reduction in the time fluctuations is expected when the amplitude of the pulses increase. In order to explore the dependency of the time resolution of the charge were studied different cases in addition to the beam test: two with cosmic rays, the one described in section 2 and another labeled as "clean room". It is important to mention that the calculation of the time resolution for the cosmic ray setup was done assuming that the resolutions of both modules are the same, i.e. the resolution is calculated according to:

$$\sigma_{total} = \sqrt{\sigma_{AD1}^2 + \sigma_{AD2}^2} \tag{6}$$

$$\sigma_{AD} = \frac{\sigma_{total}}{\sqrt{2}} \tag{7}$$

where σ_{total} is the combination of AD1 and AD2 resolutions the and σ_{AD} is the resolution of the detector.

The charges distributions were divided in slices and then obtained their corresponding time distributions. A Gaussian function was adjusted to the former and the sigma of those fits were considered as the resolution for that range of charges (slices). The gain of the PMTs on each case was set at different voltages levels, therefore the charges were normalized to their corresponding MIP position, hence the comparison was done dividing the charge and the MIP position for each case. The results are shown in the Figure 13, and as can be seen the time resolution is improved when the charge increase.

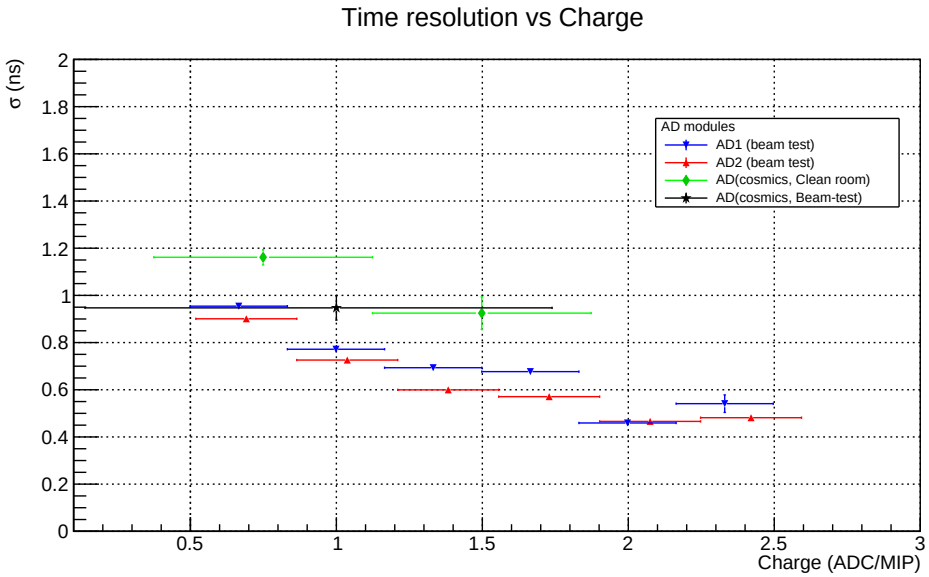

Figure 13: Charge and time resolution correlation of AD in the beam-test and measurements of cosmic rays during the preparation of the beam-test and before with a similar arrangement but in a different place (clean room).

4.3.1. Energy calibration.

Once we have estimated the energy deposition in both AD detectors we made a calibration based on this. With the measurement of the MIP position on each detector for each particle in ADC counts in the FEE, it was possible to relate its values with the theoretical calculations of the energy deposited by comparing its ratios. Table 6 contains the measured values and Table 9 the theoretical and the ratio of energy deposited with respect to ADC count. By this method it was possible to relate the MIP value in ADC counts to MeV units. The ratios for each case are consistent, taking the average of the results we obtain:

$$\varepsilon = 0.8322 \pm 0.0124 \text{ MeV/ADC} \tag{8}$$

the error is the standard deviation, the error propagation from the Table 9 is negligible (around 0.001 %).

5. Conclusions.

The performance of the detector is suitable for the purpose of its design: to have a good and homogeneous response along the plastic scintillator pad, is sensible to a minimum ionizing particle with good time resolutions. Additionally we prove that the time walk correction technique works also for 1 MIP and that the time resolution improves at higher charges. Was identified the time of travel of the photons when particles hit in the PMT photocathode, the bunch of fibers placed near to the PMT and the plastic scintillator. The consistency of the ratios between the theoretical calculation of the energy deposited and the charge measured, have allow us to obtain an energy calibration of the FEE.

Momentum*	AD1 (MeV)		AD2 (MeV)		AD1 (MeV/ADC)		AD2 (MeV/ADC)	
(MeV/c)	π^+	p^+	π^+	p^+	π^+	p^+	π^+	p^+
1000	6.69	10.89	6.68	10.95	0.838±0.003	0.820±0.002	0.823±0.003	0.805±0.014
1500	6.85	8.14	6.85	8.16	0.838±0.004	0.837±0.014	0.8107±0.005	0.821±0.0107
2000	7.00	7.25	6.99	7.26	0.862±0.002	0.824±0.006	0.838±0.002	0.816±0.006
6000	7.63	6.65	7.63	6.65	-	-	-	-

Table 9: Theoretical estimation of the energy deposition and energy per ADC count calibration in AD1 and AD2 of pions and protons and the energy ratio. *Initial momentum.